

# Wireless coverage prediction via parametric shortest paths

David Applegate  
Google Inc., USA  
dapplegate@google.com

Aaron Archer  
Google Inc., USA  
aarcher@google.com

David S. Johnson  
(deceased)

Evdokia Nikolova  
University of Texas at Austin, USA  
nikolova@austin.utexas.edu

Mikkel Thorup  
University of Copenhagen, Denmark  
mikkel2thorup@gmail.com

Ger Yang  
University of Texas at Austin, USA  
geryang@utexas.edu

## ABSTRACT

When deciding where to place access points in a wireless network, it is useful to model the signal propagation loss between a proposed antenna location and the areas it may cover. The indoor dominant path (IDP) model, introduced by Wölfle et al., is shown in the literature to have good validation and generalization error, is faster to compute than competing methods, and is used in commercial software such as WinProp, iBwave Design, and CellTrace. Previously, the algorithms known for computing it involved a worst-case exponential-time tree search, with pruning heuristics to speed it up.

We prove that the IDP model can be reduced to a parametric shortest path computation on a graph derived from the walls in the floorplan. It therefore admits a quasipolynomial-time (i.e.,  $n^{O(\log n)}$ ) algorithm. We also give a practical approximation algorithm based on running a small constant number of shortest path computations. Its provable worst-case additive error (in dB) can be made arbitrarily small via appropriate choices of parameters, and is well below 1dB for reasonable choices. We evaluate our approximation algorithm empirically against the exact IDP model, and show that it consistently beats its theoretical worst-case bounds, solving the model exactly (i.e., no error) in the vast majority of cases.

### ACM Reference Format:

David Applegate, Aaron Archer, David S. Johnson, Evdokia Nikolova, Mikkel Thorup, and Ger Yang. 2018. Wireless coverage prediction via parametric shortest paths. In *Proceedings of the Nineteenth International Symposium on Mobile Ad Hoc Networking and Computing (MobiHoc'18)*. ACM, New York, NY, USA, 12 pages. <https://doi.org/10.1145/nnnnnnnn.nnnnnnnn>

Permission to make digital or hard copies of all or part of this work for personal or classroom use is granted without fee provided that copies are not made or distributed for profit or commercial advantage and that copies bear this notice and the full citation on the first page. Copyrights for components of this work owned by others than ACM must be honored. Abstracting with credit is permitted. To copy otherwise, or republish, to post on servers or to redistribute to lists, requires prior specific permission and/or a fee. Request permissions from [permissions@acm.org](mailto:permissions@acm.org).

*MobiHoc'18, June 2018, Los Angeles, California USA*

© 2018 Association for Computing Machinery.

ACM ISBN 978-x-xxxx-xxxx-x/YY/MM. . . \$15.00

<https://doi.org/10.1145/nnnnnnnn.nnnnnnnn>

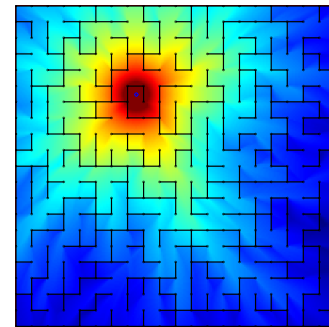


Figure 1: Heat map for a random maze.

## 1 INTRODUCTION

When installing a wireless network in an office or other building, it can be difficult to figure out the best spots to place access points (APs) in order to achieve the desired signal strength throughout the building. Wireless signal propagation is complicated, especially in an indoor office environment where the numerous walls attenuate the signal as it passes through them or diffracts around corners. Since physical trial-and-error is an expensive and time-consuming process, it would be great if we had an effective model to answer the following question: if we place an access point at location  $s$ , how strong of a signal will we receive at various other points  $t$  throughout the building? In other words, we would like to be able to produce a heat map such as in Figure 1. If we can answer this question quickly and accurately in simulation, then it opens the door to many algorithmic approaches for designing the wireless network to provide the necessary coverage, throughput, etc. that we desire.

Our original motivation for this paper came several years ago, when one of our colleagues told us that he had discovered a beautifully simple but heretical indoor radio signal propagation model in the literature, that was giving him results that accorded with reality surprisingly well. The model has two controversial features: it uses only the strongest propagation path to estimate the received signal

strength at a point, and it completely ignores paths that rely on reflections off of walls, focusing on diffractions around corners as the only mechanism for a path to change direction. This *indoor dominant path* (IDP) model lies in stark contrast to the methods blessed by conventional wisdom in the field: sophisticated ray-tracing techniques that expend a large amount of computational effort on tracing individual rays as they bounce off of multiple obstacles, and add up the contributions of multiple rays at each prediction point, accounting for phase shifting of the waves from the differential path lengths and the resulting constructive or destructive interference. Nevertheless, another member of his team was spending his days pushing a cart around the halls, measuring the actual received signal strengths from the WiFi APs in our building, and his team was finding that the IDP model matched reality roughly as well as much more sophisticated and accepted ray tracing models.

Better yet, the IDP model is fast: the commercial software he was using that featured the IDP model could compute a heat map for our entire office building from a single AP in minutes, many times faster than more sophisticated ray tracing tools. However,  $O(1\text{min})$  was still not fast enough to satisfy our colleague. For each possible AP location on a 1m grid, he wanted to compute a heat map for the entire building, also at a 1m resolution, in order to inform his AP placement. For a 60m x 60m building, this would be 3600 heat maps. At 1min apiece, this would take 2.5 days of computation. Obtaining the relevant data to fuel this modeling was a chore unto itself, and he wanted to rerun the models as the input data improved. Could we compute the model faster, he asked?

Unfortunately, we were not able to do so in time to help our colleague with his project, but we did subsequently design algorithms to compute the IDP model faster, and this paper is the result. On a synthetic 60m x 62m instance meant to model an office building (Section 5), our algorithm takes roughly 1.3sec per heat map, preceded by 2.9sec of pre-computation (which can be amortized across all of the heat maps). Using this algorithm, the full set of heat maps could be computed in under 80min, despite the fact that we have taken no particular care to produce an optimized implementation.

The main algorithmic insight of this paper is that we can reduce the IDP model to a parametric shortest path computation on an associated graph. By exploiting further structure, we can reduce this to the equivalent of about 2 ordinary, non-parametric shortest path computations on the same graph, while incurring an approximation error that is provably tiny in the worst case, and nearly always zero in practice. We call this our *geometric progression* (GP) algorithm, as it involves evaluating a geometric progression of parameter values, on geometrically increasing subsets of the original graph. Our

GP algorithm possesses two benefits over previous algorithms for the IDP model. First, it relies on fast polynomial-time algorithms for shortest path (e.g., Dijkstra's algorithm). Second, it computes path losses for *all measurement points simultaneously*. In contrast, previous algorithms for the IDP model used a worst-case exponential tree search to compute each point-to-point path loss (with pruning heuristics to speed it up), and had to do one such computation per measurement point, rather than handling them all at once.

Plets et al. published a careful study validating the IDP model, reporting superb agreement between IDP and empirical measurements on four distinct buildings with diverse physical characteristics [14]. Nevertheless, it is probably fair to say that the IDP model has not reached widespread acceptance within the academic community. Within industry, it has gained more traction, being prominently featured in at least three commercial software packages for wireless signal propagation: WinProp [2], iBwave Design [9], and CellTrace [6]. WinProp, associated with the original inventors of the indoor, outdoor, and mixed dominant path models, counts many large telecom companies and device manufacturers among its customers, including Alcatel, British Telecom, Ericsson, France Telecom, Fujitsu, Intel, Italtel, Kyocera, Motorola, Nokia, Nokia Networks, Sony, Swisscom, T-Mobile, and Vodafone [16].<sup>1</sup> In particular, Qualcomm has proved its capability of modeling femtocell performance in urban neighborhoods [7, 11], and Nokia has used it for modeling LTE multimedia broadcast systems [4]. One practical selling point of the IDP model is its insensitivity to the finer details of a building's layout [3]. Most ray tracing tools require CAD drawings or other detailed databases describing the geometry of a building, which can sometimes be impossible or prohibitively expensive to obtain. In contrast, tools like WinProp can often generate reasonable predictions based on as little as a photocopy of a floorplan, along with information on the materials that compose each wall.

Although the IDP model may not yet be fully accepted in the academic community, we take its commercial success and the strong validation results cited above as convincing indicators that it merits further study. While the community would probably value further validation of the model, that is not the aim of this paper. Here, we take the quality of the model as a given, and our goal is to present a new algorithmic approach that can solve it faster. The practical value of such a speedup is to enable new use cases such as the one described above, where our colleague wished to compute a separate heat map for each possible transmitter location in a 1m grid, to serve as input for a WiFi network planning tool.

<sup>1</sup>This customer list disappeared from WinProp's website after its acquisition by Altair [1], but we reconstructed it from the raw HTML in an archived snapshot [16].

**Our Contribution.** This paper provides faster computation of the IDP model, with rigorous approximation guarantees in worst-case polynomial running time (Section 4), in contrast to the worst-case exponential time of the existing approaches. Our *geometric progression (GP)* algorithm is also very fast in practice. While the solution it returns may (rarely) be suboptimal, it is guaranteed to be very close to optimal. The algorithm is based on a careful geometric design and analysis related to the shape of the nonlinear objective function when projected on a 2D subspace spanned by the distance and loss parameters in our problem. For reasonable parameter settings, the worst-case additive error is a fraction of 1dB (Theorems 4 and 5), and our computational experiments (Section 5) show that it actually solves the IDP model exactly (i.e., with no error) in the vast majority of cases. Under reasonable assumptions, the total running time of the GP algorithm is dominated by a single (not parametric) shortest path computation on a graph derived from the corner points of the walls in the floorplan. To sum up, GP is a fast, practical algorithm with tiny worst-case error bounds that are essentially zero in practice.

In addition, we provide a (slower but still fast) exact algorithm (Section 3), which we use to evaluate the approximation errors of the GP algorithm (Section 5). Our exact algorithm enumerates feasible paths that correspond to optimal paths in the parametric shortest path problem. The parametric problem takes two weights per edge, a distance  $d_e$  and loss  $\ell_e$ , and asks what are the shortest paths with respect to edge weights  $\ell_e + \lambda d_e$ , for all values of the parameter  $\lambda \in [0, \infty]$ . The parametric complexity refers to the number of distinct such shortest paths. The values of  $\lambda$  for which the shortest path switches from one path to another are called *breakpoints*. Our exact algorithm runs in time proportional to the number of breakpoints, so bounds on this quantity are of interest.

Carstensen constructed examples where the number of breakpoints is  $n^{\Omega(\log n)}$  [5]. Although our exact algorithm for IDP suffers from this worst-case lower bound, we do show that it has polynomial-time smoothed complexity (Theorem 6), meaning that the bad examples with  $n^{\Omega(\log n)}$  breakpoints are pathological and fragile. In our experiments, the average number of breakpoints is roughly 4 to 6 (Section 5). This means that our exact algorithm requires about 5 shortest path computations per measurement point that we wish to model, compared to GP running the equivalent of  $O(1)$  shortest path computations to closely approximate the model for *all* measurement points *simultaneously*.

**Additional Related Work.** Wölfle and Landstorfer first introduced the dominant path model in 1997 [17]. They suggested solving the model approximately (with no stated guarantees) using a heuristic grid-based method reminiscent of fast marching methods [15].

Shortly, the same authors suggested a different algorithm based on searching an exponential-sized tree, with pruning heuristics to speed it up [18]. In 1998, they also founded a company called AWE Communications to develop a highly-successful software tool called WinProp, enabling wireless coverage prediction and network design. AWE was acquired by Altair in April 2016 [1]. AWE and affiliated researchers issued a blizzard of similar conference and workshop papers, so it is difficult to choose which ones to cite, but [19] seems to be a canonical choice for the IDP model.

Multiple papers (e.g., [4, 7, 11, 14, 18, 19]) compare predictions of the dominant path model against actual physical measurements. The one by Plets et al. [14] stands out for its careful methodology and exposition. They report superb agreement between the IDP model and their empirical measurements on four distinct buildings with diverse physical characteristics, with a mean absolute modeling error of 1.29 dB on the best building and 3.08dB on the worst.

In the algorithms literature, Gusfield gave an upper bound of  $n^{O(\log n)}$  on the complexity of the parametric shortest path problem [8]. Nikolova et al. [13] gave an exact algorithm based on parametric shortest paths for a stochastic routing problem of maximizing the probability of arriving on time. Nikolova [12] later gave approximation algorithms for a general combinatorial optimization framework with several concave objective functions. At a high level, the approximation algorithms use geometric progressions similarly to our main algorithm here, but they do not apply to our problem due to a difference in objective functions and desired bounds. To wit, those algorithms provide multiplicative approximations while our algorithm gives an additive approximation requiring a different geometric analysis. In our context, a multiplicative approximation is meaningless, since path losses are measured on a log scale (dB), so the units would not even make sense for a multiplicative error. Our algorithm also provides a better tradeoff between the error and number of shortest path invocations. It remains an open question whether there exists a polynomial-time algorithm to solve the IDP exactly, but Carstensen's lower bound implies that we cannot hope to do so directly via our reduction to parametric shortest paths.

## 2 DOMINANT PATH MODEL AND REDUCTION

Ideal freespace isotropic radio signal propagation is simple: the energy received by an antenna is proportional to  $1/d^2$ , where  $d$  is the distance from the transmitter to the receiving antenna. Real-world radio signals are non-isotropic, diffract around corners, and can penetrate through or reflect off of walls. The dominant path model is motivated by a simple empirical observation: although multiple

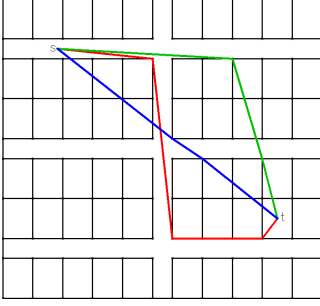


**Figure 2: Paths on convex hull for office building**

propagation paths can all contribute to the received signal strength at a measurement point  $t$ , usually the top 2 or 3 rays account for more than 95% of the energy [19]. Therefore, predicting the single path with smallest propagation loss can drive a good model of the total received signal strength. Even supposing that the dominant path contributes only 50% of the total energy, this would induce only a 3dB error, which is broadly within the range of accuracy that one achieves with more sophisticated models. The study by Plets et al. validates the IDP model that uses just the single dominant path, reporting average errors within this range.

The indoor dominant path model focuses on RF propagation inside buildings, such as for WiFi. It models the path loss  $PL(P)$  along any path  $P$ , finds the path  $P$  from source (i.e., transmitter location)  $s$  to destination  $t$  that minimizes  $PL(P)$ , and uses that number for the propagation loss from  $s$  to  $t$ . In this minimization, it considers only polygonal paths that change direction only at corner points of walls in the floorplan. Figure 2 shows examples of such paths, on a synthetic floorplan representing a generic office building.

The path loss  $PL(P)$  along path  $P$  can be broken into four components: (1) the (constant) unobstructed path loss at a reference distance  $d_0$  (typically 1m), (2) a distance term based on the ratio  $d/d_0$ , (3) penetration losses for passing through walls, and (4) diffraction losses for changing directions around obstacle corners. With the terms in this order, the formula for the path loss  $PL(P)$  (measured in dB) is:

$$PL(P) = PL_0 + 10\gamma \log_{10} \frac{d(P)}{d_0} + \sum_i WL_i + \sum_j DL_j \quad (1)$$

where the path  $P$  intersects some sequence of walls  $i$  and changes directions at some sequence of corners  $j$ . Since  $PL_0$  is a constant (40 dB at 1m [14]), we ignore it for the rest of this paper, until the experiments.

We assume throughout that the frequency of the signal is fixed. The example parameter values we state here pertain to 2.4 GHz. The wall penetration loss term  $WL_i$  is modeled as a constant for each

wall, accounting for material composition and thickness (i.e.,  $WL_i$  is given as input). Plets et al. [14] cite some typical values for thin walls, such as 2dB for glass or layered drywall, 6dB for wood, 7dB for brick, and 10dB for concrete, and for thick walls, 4dB for glass and 15dB for concrete. Note that the modeled wall penetration loss does not depend on the angle at which the path intersects the wall. The diffraction loss at corner  $j$  is modeled as the deflection angle  $\theta_j$  times some constant  $\delta_j$  that depends on the wall material at corner  $j$ . Plets et al. use  $\delta_j = 5\text{dB}/90^\circ$  for layered drywall, and  $17.5\text{dB}/90^\circ$  for concrete walls, which they determined empirically [14].

Although earlier works (e.g., [19]) used various values of  $\gamma > 2$  that were tuned to fit measurements on specific buildings, Plets et al. recommend  $\gamma = 2$ , corresponding to isotropic freespace loss, because it agrees well with their experiments and doesn't require tuning, while being simple and easy to justify theoretically. Therefore, we also use  $\gamma = 2$  in our computational experiments, although our theorems work for every choice of  $\gamma$ .

Critically, the dominant path model does *not* account for reflections. Some versions of the model incorporate other effects, such as so-called “waveguiding” along tunnels or corridors [19]. Following Plets et al. again, we eschew these extra knobs.

The heatmap in Figure 1 shows the result of solving this model for a synthetic building meant to represent a maze (see Section 5 for details). Discontinuities at each wall are obvious. A closer look also reveals “shadows” behind each corner, as the diffraction loss gradually accumulates for points whose dominant path bends around the corner.

Previous algorithms for solving the dominant path model relied on a tree search that could take exponential time in the worst case. The central theoretical contributions of this paper are to reduce the dominant path problem to a parametric shortest path problem, then give practical algorithms with rigorous guarantees to solve it.

## 2.1 Parametric shortest paths

This section defines the parametric shortest path problem in graphs, and the next section reduces the dominant path problem to it.

Our input is a graph  $G = (V, E)$  where  $V$  is a set of nodes and  $E$  is a set of edges, along with two non-negative weights on each edge  $e$ : a distance  $d_e$  and a loss  $\ell_e$ . In our context,  $d_e$  represents Euclidean distance and  $\ell_e$  represents penetration and diffraction loss. Given any parameter  $\lambda \geq 0$ , we define a *hybrid* edge weight  $h_\lambda(e) = \ell_e + \lambda d_e$ .

Fix a source node  $s \in V$  and target node  $t \in V$ , and imagine computing the shortest  $s$ - $t$  path  $P_\lambda$  in  $G$  with respect to edge weights  $h_\lambda$ , as  $\lambda$  sweeps from 0 to  $\infty$ . Note that  $P_0$  is simply the shortest path

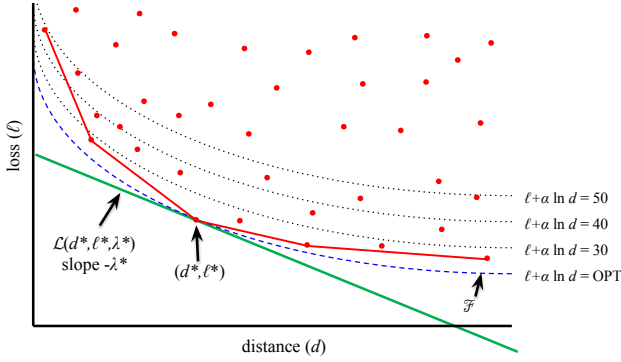


**Figure 3: Level sets and convex hull**

according to loss vector  $\ell$ , whereas  $P_\infty$  is the shortest path according to distance vector  $d$ .

Let  $(d_\lambda, \ell_\lambda)$  denote the loss and distance of path  $P_\lambda$ . There are only a finite number of possible paths, so as  $\lambda$  increases from 0 to  $\infty$ ,  $P_\lambda$  remains constant for some  $\lambda$  interval, then switches to another path at some *critical value* of  $\lambda$ , also known as a *breakpoint*. The *parametric  $s$ - $t$  shortest path problem* is to compute the full set of distinct paths  $\{P_\lambda : \lambda \in [0, \infty]\}$ , or, if we care only about their weights, then the full set of distance-loss pairs:  $\{(d_\lambda, \ell_\lambda) : \lambda \in [0, \infty]\}$ . The *parametric single-source shortest path problem* is to solve the parametric  $s$ - $t$  shortest path problem for a single  $s$  and all  $t$ .

Back to the  $s$ - $t$  version, as  $\lambda$  increases through a critical value, we always trade off a higher loss for a smaller distance. That is,  $\ell_\lambda$  increases with  $\lambda$ , and  $d_\lambda$  decreases with  $\lambda$ . We will refer often to  $d_0$  and  $d_\infty$ . To avoid confusion over the fact that  $d_0 \geq d_\infty$ , we introduce the aliases  $d_{\max} := d_0$  and  $d_{\min} := d_\infty$ . Usually, a fixed destination  $t$  will be clear from context so we suppress  $t$  in the notation as we have done above, but technically  $P_\lambda(t)$ ,  $d_\lambda(t)$ ,  $\ell_\lambda(t)$ ,  $d_{\min}(t)$  and  $d_{\max}(t)$  do depend on  $t$ .

Figure 3 visualizes what it means geometrically to minimize the function  $h_\lambda$  over all  $s$ - $t$  paths. For each of the exponentially-many  $s$ - $t$  paths  $P$ , imagine plotting the point  $(d(P), \ell(P))$  in  $\mathbb{R}^2$ . Let  $\mathcal{P}$  denote this cloud of points (i.e., the red points in Figure 3). Each level set of the function  $h_\lambda$  is a line of slope  $-\lambda$ . Place a line of slope  $-\lambda$  below the point cloud, and move it up until it first bumps into one of the points. This point corresponds to the path  $P$  that minimizes  $h_\lambda(P) = \ell(P) + \lambda d(P)$ . If we start with  $\lambda$  sufficiently high, we hit  $(d_{\min}, \ell_\infty)$ . As we lower  $\lambda$ , the optimal level set line rotates around  $(d_{\min}, \ell_\infty)$  until it hits another point in the cloud. At this value of  $\lambda$ , two paths are tied as the shortest w.r.t. edge weights  $h_\lambda$ . As  $\lambda$  decreases further, we rotate the line about this new point, until we hit a third point, and so on. By the time  $\lambda$  drops to 0, we have constructed

the lower-left convex hull of our point cloud, ending at  $(d_{\max}, \ell_0)$  (i.e., the red polyline in Figure 3).

The corner points (extreme points) of this convex hull correspond to the paths output by the parametric shortest path computation. To avoid confusion with the corners of walls, we will henceforth refer to the corners of the convex hull as *extreme points*. The three paths shown in Figure 2 are in fact paths that correspond to extreme points for the  $s$ - $t$  pair shown. These extreme points partition the  $\lambda$  range  $[0, \infty]$  into segments, where each extreme point represents the shortest path w.r.t.  $h_\lambda$  for all  $\lambda$  in its segment. The boundary points between these segments represent the critical values of  $\lambda$ , which correspond to (the negative of) the slopes of the red line segments in Figure 3. These facts will be important for understanding both our geometric progression algorithm (Section 4) and some of our experimental results (Section 5).

## 2.2 A graph representing all valid paths

This section constructs a graph with two weight functions  $d$  and  $\ell$  that capture the distance and (penetration loss + diffraction loss) of paths in the dominant path model. We must define a graph  $G$  and edge weights  $d_e$  and  $\ell_e$  such that:

- (1) the distance  $d(P)$  and loss  $\ell(P)$  of path  $P$  in the dominant path model equal  $\sum_{e \in P} d_e$  and  $\sum_{e \in P} \ell_e$ , and
- (2) every valid physical path  $P$  in the dominant path model corresponds to a path in the graph,
- (3) every undominated path in the graph corresponds to a physical path that is considered in the dominant path model.

We construct such a graph in two phases: first a graph  $G_1$  that encodes all relevant paths, plus their distances and wall penetration losses, then a related graph  $G_2$  that also encodes diffraction losses.

Constructing  $G_1 = (V_1, E_1)$  is straightforward. The node set  $V_1$  is the union of three sets: the single source  $\{s\}$ , the set of  $T$  destinations (aka *measurement points*), and the set of *corners*  $C$ . Here,  $T$  means the set of all points for which we wish to compute the dominant path, and  $C$  means the set of endpoints of wall segments in the floor plan. The set  $E_1$  is the union of four sets of directed edges: all  $s - C$ ,  $s - T$ ,  $C - C$ , and  $C - T$  pairs. There is no need for  $T - T$  edges, since all intermediate points in the polygonal  $s$ - $t$  paths considered in the dominant path model are corner points. For each  $e \in E_1$ , set  $d_e$  to the Euclidean distance between its endpoints, and  $\ell_e$  to the sum of the penetration losses of all walls it crosses.

There are two defects in  $G_1$  that we must correct in our construction of  $G_2$ : it models neither the penetration losses at corners nor the diffraction losses. We solve this problem by “exploding” each corner node  $c \in C$ , replacing it with a set of new nodes, one for each

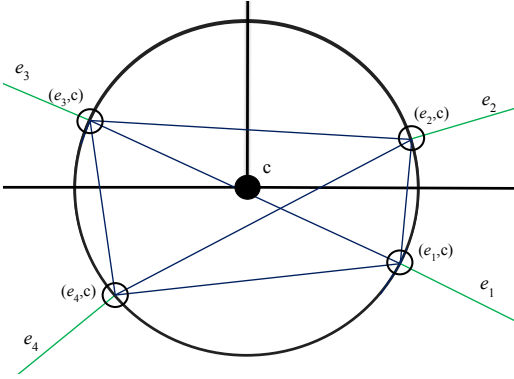


Figure 4:  $G_2$  corner

incoming and outgoing edge  $e$ . These new nodes are *directed sockets* of  $G_1$ , i.e., ordered pairs  $(e, c)$  where  $e \in E_1$  is incident to  $c$  in  $G_1$ . These new socket nodes are illustrated by the circles in Figure 4, labeled  $(e_1, c), \dots, (e_4, c)$ . We now add a directed edge from each incoming socket to each outgoing socket at corner  $c$ , represented by the six blue edges inside the big circle in Figure 4.

For a new intra-cluster edge  $e \in E_2$  that runs from incoming socket  $(e_1, c)$  to outgoing socket  $(e_2, c)$ ,  $d_e = 0$  as this edge covers zero physical distance. The loss  $\ell_e$  is the sum of two terms: one for the diffraction loss, and one for the penetration loss. The diffraction loss is  $\delta_c \theta_{e_1, e_2}$ , where  $\theta_{e_1, e_2}$  is the physical angle between directed edges  $e_1$  and  $e_2$ . For the penetration loss, we consider the total loss for the walls incident at corner  $c$  encountered as we sweep either clockwise or counterclockwise from  $e_1$  to  $e_2$ , and take the minimum.

There are two more subtleties. First, there will be edges of  $G_1$  that run from one end of a wall segment to the other. We must actually represent these as two edges, one on each side of the wall, so that we can compute the penetration losses correctly in the intra-corner edges of  $G_2$ . Second, sets of co-linear corner points are a common occurrence in buildings, so we cannot assume away their existence. It would be problematic to consider edges directly from one end of the line of corners to the other, because we would have to make a decision at each intermediate corner point about which side of the wall the edge lies on for that segment, thereby introducing an exponential number of parallel edges. Instead, we simply delete these edges, keeping only the edges connecting adjacent pairs along the line of corner points.

It is clear that every valid path  $P$  in the dominant path model is represented by a corresponding path in  $G_2$ , and  $d(P)$  and  $\ell(P)$  as defined by  $G_2$  agree with the values assigned by the dominant path model. Conversely, every path in  $G_2$  that visits each corner point at most once corresponds to a valid path. There also exist paths  $P$  in  $G_2$

that visit a corner point more than once via different sockets from  $G_1$ , which are technically different nodes in  $G_2$  and hence do not violate the definition of a path being a trail with no cycles. However, it is easily seen that those paths are always dominated by paths that do not revisit corners.

To sum up, for each path  $P$  considered valid by the dominant path model, there is a corresponding path  $P$  in  $G_2$ , and we have set the edge weights in  $G_2$  such that (1) becomes

$$PL(P) = PL_0 + \ell(P) + 10\gamma \log_{10} d(P) \quad (2)$$

Moreover, all non-valid paths in  $G_2$  are irrelevant. To make this mathematically cleaner, we transform the  $\log_{10}$  to  $\ln$ , plug in the freespace loss value of  $\gamma = 2$ , and define  $\alpha = \frac{10\gamma}{\ln 10} \text{dB} \approx 8.686 \text{dB}$ . We also define  $f(d, \ell) = \ell + \alpha \ln d$ , and  $f(P) = f(d(P), \ell(P))$ . With these transformations, the dominant path is the path  $P$  that minimizes  $f(P)$ .

### 2.3 Reduction to parametric shortest path

This section demonstrates that the dominant  $s$ - $t$  path is one of the parametric shortest  $s$ - $t$  paths in  $G_2$ .

Suppose  $P^*$  is the dominant  $s$ - $t$  path, and define  $d^* = d(P^*)$ ,  $\ell^* = \ell(P^*)$ , and  $\lambda^* = \alpha/d^*$ . We devote the rest of this section to proving the following theorem:

**THEOREM 1.** Define  $d^* = d(P^*)$ ,  $\lambda^* = \frac{\alpha}{d^*}$  where  $P^*$  is the dominant  $s$ - $t$  path. Then  $P^*$  is also the  $P$  that minimizes  $h_{\lambda^*}(P) = \ell(P) + \lambda^* d(P)$ .

We introduce some notation to set up the proof. The solution to the parametric  $s$ - $t$  shortest path problem yields  $\{P_\lambda : \lambda \in [0, \infty]\}$  and their corresponding distance-loss pairs  $\{(d_\lambda, \ell_\lambda) : \lambda \in [0, \infty]\}$ . These are actually finite sets, one per critical value of  $\lambda$ , so we can simply evaluate  $\ell + \alpha \ln d$  for each of these  $(d, \ell)$  pairs, and select the smallest one. Since  $(d_\lambda^*, \ell_\lambda^*)$  is one of these pairs, and Theorem 1 says that it is the dominant path, this solves the dominant path model.

To finish the reduction, we just need to prove Theorem 1. This is surprisingly simple, as illustrated in Figure 5. First, we define  $\mathcal{L}(d, \ell, \lambda)$  to be the line through  $(d, \ell)$  of slope  $-\lambda$ .

**Proof:** As in Section 2.1, imagine the point cloud  $\mathcal{P}$  of  $(d(P), \ell(P))$  pairs, for all paths  $P$ . Let  $\ell^* = \ell(P^*)$  and  $OPT = f(d^*, \ell^*) = \ell^* + \alpha \ln d^*$  and consider the level curve  $\mathcal{F} := \{(d, \ell) : \ell = OPT - \alpha \ln d\}$  of  $f$  running through  $(d^*, \ell^*)$ . Because  $P^*$  is the optimal path, the rest of  $\mathcal{P}$  lies on or above this level curve. Because  $\ln d$  is a concave function of  $d$ , this level curve is convex, and it therefore has a supporting tangent line  $\mathcal{L}(d^*, \ell^*, \lambda^*)$  at  $(d^*, \ell^*)$  of slope  $-\lambda^* = -\frac{\alpha}{d^*}$  (aka the derivative of the level curve at  $d^*$ ), which is a level set for  $h_\lambda$ . The point  $(d^*, \ell^*)$  minimizes  $h_{\lambda^*}$  because the  $\mathcal{L}(d^*, \ell^*, \lambda^*)$

passes through  $(d^*, \ell^*)$ , the rest of  $\mathcal{F}$  lies strictly above the tangent line, and the rest of  $\mathcal{P}$  lies strictly above  $\mathcal{F}$ . ■

We note that a similar theorem and proof would work if  $\ln d$  were replaced by any other concave function of  $d$ .

### 3 EXACT CONVEX HULL

By the results of Section 2, solving the  $s$ - $t$  dominant path model reduces to a parametric  $s$ - $t$  shortest path computation, or equivalently finding the lower left convex hull of the point cloud  $\mathcal{P}$ . Let  $\text{SP}(\lambda)$  denote the shortest path calculation w.r.t. edge weights  $h_\lambda$ . We now prove the following theorem:

**THEOREM 2.** *The parametric  $s$ - $t$  shortest path problem can be solved using  $2k - 1$   $s$ - $t$  shortest path computations, where  $k$  is the number of extreme points, including both endpoints.*

**Proof:** Recall that  $\text{SP}(\infty)$  yields the leftmost point in the convex hull,  $(d_{\min}, \ell_\infty)$ , whereas  $\text{SP}(0)$  yields the rightmost point,  $(d_{\max}, \ell_0)$ . Next, set  $\lambda = (\ell_\infty - \ell_0)/(d_{\max} - d_{\min})$  and compute  $\text{SP}(\lambda)$ . One of two things happens. If  $(d_{\min}, \ell_\infty)$  and  $(d_{\max}, \ell_0)$  are the only points on the convex hull, then  $\text{SP}(\lambda)$  will return one of these two points, proving that all other points lie on or above the line  $\mathcal{L}(d_{\min}, \ell_\infty, \lambda)$ , so we are done. Otherwise, it will return some point  $(d, \ell)$  below this line. In that case, we continue constructing the convex hull recursively on each of the two intervals  $[d_{\min}, d]$  and  $[d, d_{\max}]$ . Every value of  $\lambda$  we try either discovers a new extreme point or proves that the segment connecting the extreme points at either end of the current interval is indeed a facet of the convex hull. Therefore, the number of shortest path computations is  $k + (k - 1) = 2k - 1$ . ■

As noted in [8],  $k$  is at most  $n^{O(\log n)}$ . Therefore, the parametric  $s$ - $t$  shortest path problem can be solved using at most  $n^{O(\log n)}$  shortest path computations.

### 4 GEOMETRIC PROGRESSION

From Theorem 2, we can compute an  $s$ - $t$  dominant path efficiently as long as the number of breakpoints is small. This observation drives our smoothed analysis in Section 7. However, if we wish to compute dominant paths from a single source  $s$  to all destinations then we can do much better, especially if we are willing to tolerate a small additive approximation error. Our *geometric progression* (GP) algorithm does precisely this. We devote this section to its definition, then to analyzing its approximation error and practical time complexity.

Given fixed numbers  $r > 1$  and  $\lambda_0 > 0$ , define a geometric progression of parameter values  $\lambda_i = \lambda_0 r^i$  for  $i \in \mathbb{Z}$ . It is safe to think of  $r$  as 2. The geometric progression algorithm  $\text{GP}(r, \lambda_0)$  runs

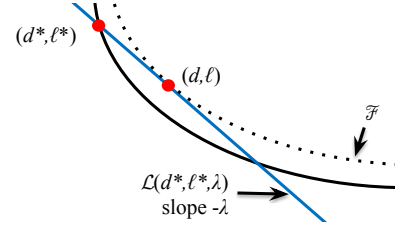


**Figure 5: Approximation bound**

$\text{SP}(\lambda_i)$  for  $\lambda_i$  in some sufficiently wide range (that we specify later). For each destination point  $t$ , it then outputs the best of the  $s$ - $t$  paths  $P$  it found, according to the real objective function  $f$ . Since our algorithm always outputs the path loss of some valid path, it never underestimates the optimal path loss.

For each  $t$ , Theorem 1 guarantees there is some  $\lambda$  such that  $\text{SP}(\lambda)$  finds the dominant  $s$ - $t$  path. Although we don't know which  $\lambda$  that is, the  $\text{GP}(r, \lambda_0)$  algorithm is guaranteed to use some nearby value, and this allows us to bound our error, as shown by Theorems 3, 4 and 5.

**THEOREM 3.** *If  $(d^*, \ell^*)$  is the optimal distance-loss for destination point  $t$  and  $\lambda^* = \alpha/d^*$ , then  $\text{SP}(\lambda)$  with  $\lambda = \beta\lambda^*$  yields a path loss  $f(d_\lambda, \ell_\lambda) \leq f(d^*, \ell^*) + \alpha(-1 + \beta - \ln \beta)$ .*

It turns out that  $\hat{\beta} := \frac{r \ln r}{r-1}$  is the worst value of  $\beta$ .

**THEOREM 4.** *If  $(d^*, \ell^*)$  is the distance-loss for the dominant path to destination  $t$ , then algorithm  $\text{GP}(r, \lambda_0)$  returns an  $s$ - $t$  path  $P$  with  $f(P) \leq f(d^*, \ell^*) + \alpha(-1 + \frac{\ln r}{r-1} + \ln(r-1) - \ln \ln r)$  dB.*

**THEOREM 5.** *Set  $\lambda_0 = r^u$  where  $u$  is chosen randomly from the distribution  $U(0, 1)$ . Then for each destination  $t$ , algorithm  $\text{GP}(r, \lambda_0)$  returns an  $s$ - $t$  path  $P$  with  $E[f(P)] \leq f(d^*, \ell^*) + \alpha(-\frac{1}{2} \ln r + \ln(r-1) - \ln \ln r)$  dB, where  $(d^*, \ell^*)$  is the distance-loss of the dominant path.*

Note that the expectation in Theorem 5 is w.r.t. the random choice of  $u$ , whereas the input is assumed to be adversarial. As we prove these theorems, some of our intermediate results will tell us what range of  $\lambda_i$  we must consider, and also allow us to prune  $G_2$  before running each  $\text{SP}(\lambda_i)$  calculation. In particular, each measurement point appears in only a small number of these graphs,  $O(1)$  in practice.

**Proof of Theorem 3:** The following geometric argument is illustrated in Figure 5. Since  $\text{SP}(\lambda)$  minimizes  $h_\lambda$ , we know  $h_\lambda(d_\lambda, \ell_\lambda) \leq h_\lambda(d^*, \ell^*)$ . Hence,  $(d_\lambda, \ell_\lambda)$  must lie on or below the line  $\mathcal{L}(d^*, \ell^*, \lambda)$ , the level set for  $h_\lambda$  through  $(d^*, \ell^*)$ . Among all such points, the one that maximizes  $f$  occurs at the point of tangency between  $\mathcal{L}(d^*, \ell^*, \lambda)$  and some level curve  $\mathcal{F}$  of  $f$ . There is only one such

point of tangency, which occurs at  $d = \alpha/\lambda$ ,  $\ell = \ell^* - \lambda(d - d^*)$ . We upper bound  $f(d_\lambda, \ell_\lambda)$  by  $f(d, \ell)$ .

$$\begin{aligned} f(d_\lambda, \ell_\lambda) &\leq f(d, \ell) = f(d^*, \ell^*) + (f(d, \ell) - f(d^*, \ell^*)) \\ &= f(d^*, \ell^*) + (\ell - \ell^*) + \alpha \ln(d/d^*) \\ &= f(d^*, \ell^*) - \lambda(d - d^*) - \alpha \ln \beta \\ &= f(d^*, \ell^*) - \lambda(\alpha/\lambda - \alpha/\lambda^*) - \alpha \ln \beta \\ &= f(d^*, \ell^*) + \alpha(-1 + \beta - \ln \beta) \end{aligned}$$

■

**Proof of Theorem 4:** Let  $\lambda^* = \alpha/d^*$ . Because consecutive  $\lambda_i$  are spaced by a multiplicative  $r$ , one of them (call it  $\lambda_{\text{lo}}$ ) must land in the range  $[\frac{1}{r}\lambda^*, \lambda^*]$ , and one (call it  $\lambda_{\text{hi}}$ ) must land in the range  $[\lambda^*, r\lambda^*]$ . Thus,  $\lambda_{\text{hi}} = \beta\lambda^*$  and  $\lambda_{\text{lo}} = \frac{\beta}{r}\lambda^*$  for some  $\beta \in [1, r]$ . Applying our upper bound from Theorem 3 twice, we see that the path  $P$  returned by  $GP(r, \lambda_0)$  has error at most

$$\alpha(-1 + \min(\beta - \ln \beta, \beta/r - \ln \beta/r))$$

This min is maximized at  $\beta = \hat{\beta}$ , where the two terms in the min are both equal to

$$\frac{r \ln r}{r-1} + \ln\left(\frac{r \ln r}{r-1}\right) = \frac{\ln r}{r-1} + \ln(r-1) - \ln \ln r$$

The desired bound follows. ■

**Proof of Theorem 5:** Define  $\lambda_{\text{lo}}$  and  $\lambda_{\text{hi}}$  as in the proof of Theorem 4:  $\lambda_{\text{lo}} = \frac{\beta}{r}\lambda^*$ ,  $\lambda_{\text{hi}} = \beta\lambda^*$ , for some  $\beta \in [1, r]$ . Because  $\log_r \lambda_0 = u \sim U(0, 1)$ , we have  $\beta \sim r^{U(0,1)}$ . Apply the bound from Theorem 3 twice, using the bound from  $\lambda_{\text{hi}}$  for  $\beta \leq \hat{\beta}$  and the bound from  $\lambda_{\text{lo}}$  for  $\beta \geq \hat{\beta}$ . Let  $\hat{u} = \ln_r \hat{\beta}$ . Then, in expectation, the better of these two bounds is:

$$-\alpha + \alpha \left( \int_0^{\hat{u}} (r^u - \ln r^u) du + \int_{\hat{u}}^1 (r^{u-1} - \ln r^{u-1}) du \right) \quad (3)$$

The first integral simplifies to

$$\frac{r}{r-1} - \frac{1}{\ln r} - \frac{1}{2} \hat{u}^2 \ln r$$

and the second simplifies to

$$\frac{1}{\ln r} - \frac{1}{r-1} + (1 - \hat{u}) \ln r - \frac{1}{2} (1 - \hat{u}^2) \ln r$$

Summing these gives  $1 + \frac{1}{2} \ln r - \hat{u} \ln r$ . Plugging this back into (3) gives the promised bound. ■

These bounds are quite tight, even for generous values of  $r$ . For instance, when  $r = 2$ , the worst-case error from Theorem 4 is only 0.5182 dB, and our upper bound on the expected error is a mere 0.1732 dB. These errors are dwarfed by the validation errors of the model itself, as reported in Plets et al. [14], which are mostly in the 1dB to 5dB range.

## 4.1 Practical considerations

We have one piece of unfinished business, which is to define the range of  $\lambda_i$  values for which  $GP(r, \lambda_0)$  must run the  $SP(\lambda_i)$  computation. In addition, we shall demonstrate some pruning tricks on  $G_2$  which imply, under some reasonable assumptions, that the total running time of all of our  $SP(\lambda_i)$  computations is  $O(1)$  times the cost of running Dijkstra just once on  $G_2$ . Finally, we discuss how to save time and memory by running Dijkstra on  $G_2$  implicitly, while explicitly constructing only  $G_1$  (and not  $G_2$ ) in memory.

**4.1.1 Pruning  $G_2$ .** Let us fix a particular destination  $t$ , and set

$$I_{\lambda^*} = \left[ \frac{\hat{\beta}}{r} \lambda^*, \hat{\beta} \lambda^* \right].$$

The proofs of Theorems 4 and 5 rely only on running  $SP(\lambda)$  for some  $\lambda \in I_{\lambda^*}$ . Although we do not know  $d^*$  or  $\lambda^* = \alpha/d^*$ , we do know that  $\lambda^* \in [\frac{\alpha}{d_{\max}}, \frac{\alpha}{d_{\min}}]$ . Therefore, if we run  $SP(\lambda_i)$  for each of the  $\lambda_i$  in

$$I(t) := \bigcup_{\lambda^* \in [\frac{\alpha}{d_{\max}}, \frac{\alpha}{d_{\min}}]} I_{\lambda^*} = \left[ \frac{\alpha \hat{\beta}}{r d_{\max}}, \frac{\alpha \hat{\beta}}{d_{\min}} \right] \quad (4)$$

then we satisfy the error bounds in Theorems 4 and 5. Therefore, for each  $\lambda_i$  considered in algorithm  $GP(r, \lambda_0)$ , we need to include node  $t$  in  $G_2$  only for the destinations

$$\begin{aligned} M(\lambda_i) &:= \{t : \lambda_i \in I(t)\} \\ &= \left\{ t : d_{\min}(t) \leq \frac{\alpha \hat{\beta}}{\lambda_i} \text{ and } d_{\max}(t) \geq \frac{\alpha \hat{\beta}}{r \lambda_i} \right\}. \end{aligned}$$

In particular, if  $M(\lambda_i) = \emptyset$ , then we do not have to run  $SP(\lambda_i)$  at all.

When we first defined  $GP(r, \lambda_0)$ , we deferred the question of which  $SP(\lambda_i)$  computations are necessary. Let us define  $D_{\min} = \min_t d_{\min}(t)$  and  $D_{\max} = \max_t d_{\max}(t)$ . Then we must do all  $\lambda_i$  in  $[\frac{\alpha \hat{\beta}}{r D_{\max}}, \frac{\alpha \hat{\beta}}{D_{\min}}]$ .

The multiplicative width of  $I(t)$  is only  $r \frac{d_{\max}}{d_{\min}}$ , so in expectation, each destination  $t$  is pruned from  $G_2$  for all but  $\log_r \frac{r d_{\max}(t)}{d_{\min}(t)}$  values of  $\lambda_i$ . Recall that  $d_{\min}(t)$  is merely the straight-line distance from  $s$  to  $t$ , whereas  $d_{\max}(t)$  is the distance along the  $s$ - $t$  path  $P_0$  with lowest (penetration + diffraction) losses. Since the diffraction losses are relatively high compared to the penetration losses, e.g., for dry-wall, a 90° turn costs the same as penetrating 2.5 walls (Section 2). Therefore, we would expect that path  $P_0$  does not bend too much, and therefore  $\frac{d_{\max}(t)}{d_{\min}(t)}$  will be fairly small in practice, typically less than 2. In this case, if using  $r = 2$ , then we include most destinations  $t$  in only one or two of the  $SP(\lambda)$  computations.

We can also prune some of the corner points from  $G_2$ . If the distance  $d(s, c) + d(c, t)$  from  $s$  straight to corner point  $c \in C$  straight to  $t$  exceeds  $d_{\max}(t)$ , then we need not consider any  $s$ - $t$  paths that

go through  $c$ , because they will be both longer than  $P_0(t)$  and have equal or greater loss than  $P_0(t)$  (which has minimum loss over all  $s$ - $t$  paths). In this case, we may prune the edge  $(c, t)$  from  $G_2$ . In addition, if this condition holds for all  $t \in M(\lambda_i)$ , then we prune  $c$  from  $G_2$  entirely.

Conceptually, our sequence of  $SP(\lambda_i)$  computations is performed on a single graph,  $G_2$ . However, the pruning operations that we just discussed shrink it greatly for most values of  $\lambda_i$ , because of the geometry. Let us sweep  $\lambda$  downward from  $\frac{\alpha\hat{\beta}}{D_{\min}}$  down to  $\frac{\alpha\hat{\beta}}{rD_{\max}}$ . Initially, only the nodes close to the source  $s$  remain unpruned. Each time we divide  $\lambda$  by  $r$ , the outer radius of the annulus of measurement points defining  $M(\lambda)$  grows by a factor of  $r$ . Assuming the ratio  $\frac{d_{\max}(t)}{d_{\min}(t)}$  is  $O(1)$ , then the inner radius of this annulus also grows by roughly a factor of  $r$ . In the typical case, the set of measurement points is a uniform grid, which means that  $|M(\lambda)|$  grows by roughly a factor of  $r^2$ . If the corners are also spaced relatively uniformly, then the number of unpruned corners also grows by roughly  $r^2$ . Therefore, the set of relevant unpruned  $C-C$  and  $C-T$  edges grows by roughly  $r^4$ . Therefore, the total cost of all of the  $SP(\lambda_i)$  computations is dominated by the ones at the end of the process (small  $\lambda_i$ ), where the pruned version of  $G_2$  is the largest, and by  $SP(0)$ , which is used to compute  $d_{\max}(t)$  for all  $t$  and so must run on the full  $G_2$ .

**4.1.2 Running Dijkstra on  $G_2$  implicitly.** Recall Dijkstra's shortest path algorithm [10]. We maintain a distance label  $L_v$  on each node  $v$ , initialized to 0 for  $s$  and  $\infty$  for all other nodes, with all labels *active*. At each step, we select the smallest active label, make it inactive (aka *finalize* it), and *relax* each of its outgoing edges  $e = (v, w)$ , meaning that we update  $L_w \leftarrow \min(L_w, L_v + w_e)$ . Once the last label is finalized,  $L_v$  is the weight of the shortest path from  $s$  to  $v$ .

Recall that most of the nodes in  $G_2$  are sockets  $(e, c)$  from  $G_1$ , where  $c \in C$  is a corner point with incident edge  $e$ , and most of the edges of  $G_2$  are the intra-corner edges from each incoming socket to each outgoing socket at  $c$ . We can save a huge amount of memory by explicitly constructing and storing only  $G_1$ , and running Dijkstra implicitly on  $G_2$ . To do this, we maintain our distance labels  $L$  on the sockets of  $G_1$ . When we finalize the label of an incoming socket  $(e, c)$ , we must relax all of its outgoing intra-corner edges to the outgoing sockets  $(e', c)$ . But the cost of each of these edges is a function of just three things: (1) the diffraction angle between  $e$  and  $e'$ , (2) the sector of  $e$ , and (3) the sector of  $e'$ , where *sector* refers to the directions between two consecutive walls meeting at  $c$ . The pair of sectors determines the penetration loss and the deflection angle determines the diffraction loss.

This explains how to run Dijkstra without ever storing  $G_2$ . Better yet, we can actually avoid the vast majority of no-op relaxations (i.e., ones that do not actually update their label). This is because, for all outgoing sockets  $(e', c)$  within a given sector, the penetration loss from  $(e, c)$  is the same, and the diffraction loss, plotted as a function of the angle  $\theta$  is a line with constant slope equal to  $\pm\delta_c$ , the diffraction constant at corner  $c$ . Thus, we can visualize each of the finalized incoming sockets  $(e, c)$  at corner  $c$  as inducing either a V-shape (for its own and its opposite sector) or a line (for all other sectors), representing the implied path weight to a hypothetical outgoing socket at angle  $\theta$ . The actual Dijkstra label will be the minimum of these lines and V-shapes.

To actually perform the relaxation for a newly-finalized incoming socket  $(e, c)$ , we start in the opposite sector at angle 0, the bottom of the V, and march through the outgoing sockets in clockwise order to  $180^\circ$ , then do it again counterclockwise. If we ever encounter an angle at which our implied label exceeds the existing label (aka a no-op relaxation), we know that our line is dominated for the rest of that sector, since we are increasing at rate  $\delta_c$  and all other lines are increasing or decreasing at that same rate. We then pick up at the next sector, where we have a chance again because the vertical offset of each line is different (from the differing penetration losses, depending on the sector of the corresponding incoming socket). Therefore, the number of no-op Dijkstra relaxations that we must perform is bounded by the number of sectors + 2 (since the  $0^\circ$  and  $180^\circ$  sectors each count twice).

## 5 EXPERIMENTS

**Datasets:** For our experiments, we consider two types of artificial "buildings." These are not meant to replicate real buildings, but rather just to exhibit some properties of our algorithms. The first type are ten random "maze" buildings, like the one shown in Figure 1. These are formed by taking a 20x20 grid graph, removing a random spanning tree, and then taking the planar dual, leaving a 20x20 connected maze of 3m x 3m cells. This gives 60m x 60m buildings, with 441 corner points, 441 walls, and 3600 measurement points (on a 1m grid). The second building is an artificial office building, like the one shown in Figure 2, to contrast with the random mazes. Although this is not a real office building, it does provide a check that the experimental results are not purely an artifact of the random mazes. It consists of a very regular grid of 3m x 4m offices connected by 2m wide hallways, with 12 rows of 20 offices each (where Figure 2 shows just a portion with 6 rows of 10 offices). This office is 62m x 60m, with 418 corner points, 658 walls, and 3720 measurement

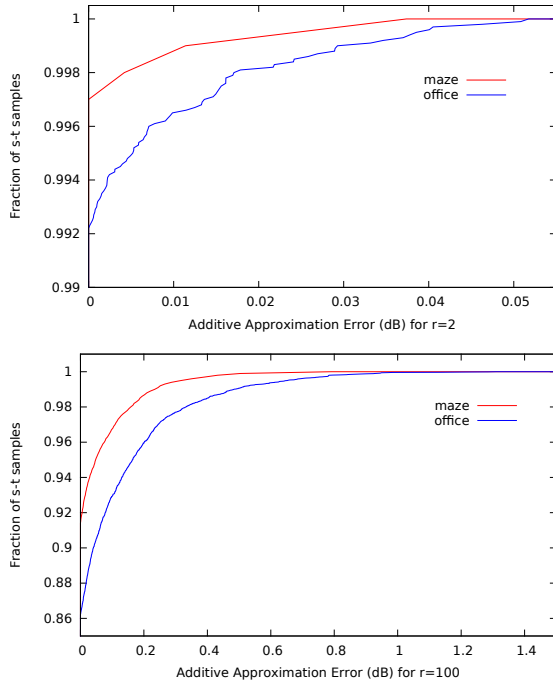


Figure 6: Error distributions for  $r = 2$  and  $r = 100$

points (on a 1m grid). For both types of artificial buildings, the exterior walls are concrete (with 15.0dB penetration loss), the interior walls are layered drywall (with 2.0dB penetration loss), and the diffraction loss at all corners is 5.0dB/90° (loss values from Plets et al. [14]). Of course, our algorithms work just fine with different loss parameters for each wall and corner, but uniform values are most easily justified.

**Approximation errors:** First, we consider the approximation error of the GP algorithm from Section 4. For each of the ten random mazes, we sampled 1000 random source-destination pairs, and for the office building, we sampled 10,000 random pairs. For each pair we computed the full convex hull of parametric shortest paths (Section 3). Even though Carstensen [5] gives a worst-case lower bound of  $n^{\Omega(\log n)}$  for the number of extreme points on the convex hull, the worst case we encountered was 19 extreme points, and the mean was only 4.2 for the mazes, and 5.5 for the office building.

Based on these convex hulls, we compute the exact solution to the IDP model, which allows us to compute the expected error for each source/destination pair in the GP approximation algorithm. All expectations are w.r.t. the random choice of  $\lambda_0$  in  $GP(r, \lambda_0)$ . Figure 6 shows the error distributions for  $r = 2$  and  $r = 100$ . Recall that our errors are one-sided: we can only overestimate the path loss of the dominant path. The actual expected errors are much better than the

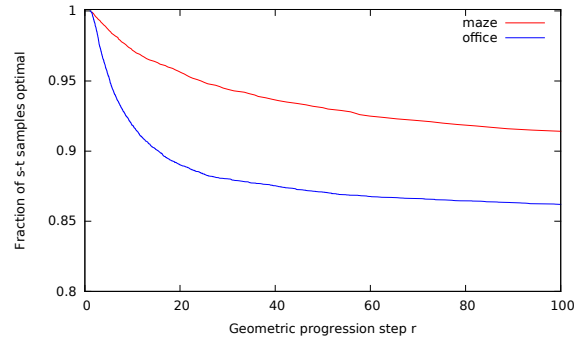


Figure 7: Frequency of identification of dominant  $s-t$  path

bounds from Theorems 4 and 5. For instance, with  $r = 2$ , the GP algorithm failed to find the exact dominant  $s-t$  path for fewer than 0.8% of the  $s-t$  pairs, and the error exceeded 0.06dB for none of them. These approximation errors are insignificant compared to the model validation errors of 1dB to 5dB reported by Plets et al. [14]. Even for the extreme case of  $r = 100$ , for which Theorem 5 gives an expected error bound of 6.6dB, the worst observed error is only 1.5dB and 99% of the  $s-t$  pairs have error below 0.6dB. There is never any reason to use such a large value of  $r$ ; we show it just to emphasize that our results are extremely robust to  $r$ .

To understand why the geometric progression algorithm actually finds the dominant  $s-t$  path so frequently, consider the two break-points  $\lambda_{l_0}$  and  $\lambda_{h_i}$  corresponding to the two segments of the convex hull adjacent to the extreme point representing the dominant  $s-t$  path (Figure 3). The dominant  $s-t$  path will be returned by  $SP(\lambda)$  for every value of  $\lambda \in (\lambda_{l_0}, \lambda_{h_i})$ . In particular, if  $\lambda_{h_i}/\lambda_{l_0} > r$ , then the geometric progression is *guaranteed* to have  $\lambda_i \in (\lambda_{l_0}, \lambda_{h_i})$  for some  $i$ , and hence find the dominant  $s-t$  path. Figure 7 shows, as a function of  $r$ , how often we are guaranteed to find the dominant  $s-t$  path, i.e., what fraction of our sampled  $s-t$  pairs satisfy  $\lambda_{h_i}/\lambda_{l_0} > r$ .

**Pruning  $G_2$  :** As observed in Section 4.1.1, a measurement point  $t$  needs to be included when running  $SP(\lambda_i)$  only for each  $\lambda_i \in I(t)$ , so is pruned from  $G_2$  for all but  $\log_r \frac{rd_{\max}(t)}{d_{\min}(t)}$  values of  $\lambda_i$  (in expectation). To evaluate how effective this pruning was, we considered  $r = 2$  for ten random choices of  $s$  and a 1m grid of measurement points for each of ten random maze buildings and the office building. For the random maze buildings, the expected number of  $SP(\lambda_i)$  computations that left the average measurement point unpruned was only 1.06, and the maximum expectation we encountered over all measurement points was only 2.14. For the office building, the long straight hallways result in higher  $\frac{d_{\max}(t)}{d_{\min}(t)}$  ratios, but still the average number of  $SP(\lambda_i)$  a measurement point was included in was only 1.29, and the maximum we encountered

was only 2.69. Hence, the total complexity of the full  $GP(2, \lambda_0)$  algorithm is very close to the complexity of running two Dijkstra computations on the unpruned version of  $gTwo$ : one with  $\lambda = 0$  to compute  $d_{\max}(t)$  for all  $t$ , and the sequence of Dijkstra runs on pruned versions of  $gTwo$  add up to about one additional Dijkstra on the full  $G_2$ .

**Implicit  $G_2$  savings:** A key implementation detail is to avoid no-op Dijkstra edge relaxations on the implicit representation of  $G_2$  (Section 4.1.2). In the run that generated the heat map in Figure 1, roughly 99% of the relaxations were no-ops, so this trick allowed us to perform only  $2.18 \times 10^8$  relaxation steps rather than  $2.87 \times 10^{10}$ .

**Running time:** For the mazes, building  $G_2$  took 3.0 CPU sec, and generating a heat map from a single source took 1.0sec. For the office, building  $G_2$  took 2.9sec, and a single heat map took 1.3sec. The experiments were run using a single thread on a 3.6GHz Intel Xeon E5-1650v4 CPU.

## 6 SMOOTHED ANALYSIS

The exact algorithm runs fast in simulations, despite its worst-case super polynomial running time in theory. The good practical performance can be explained theoretically by smoothed analysis: the idea that the worst-case instances are rare and most likely in practice the algorithm encounters “good” instances, for which the number of breakpoints (and hence also the number of extreme points) that are enumerated by the exact algorithm, is small. We state this result informally, then follow up with a rigorous development.

**THEOREM 6.** *The exact IDP model can be solved in smoothed polynomial time.*

Formally, the smoothed analysis framework defines a perturbation of the input (the edge weight vectors  $d, \ell \in \mathbb{R}^m$ , where  $m$  is the number of edges in the graph) and proves that in expectation with respect to this perturbation, the algorithm running time (specifically, the number of extreme points), is polynomial.

To help us state the smoothed bound, we first note that the optimal path is an extreme point of the flow polytope  $P \in \mathbb{R}^m$ , defined via the standard flow constraints:

$$\begin{aligned} \sum_{e \text{ out of } v} x_e &= \sum_{e \text{ into } v} x_e && \text{for each node } v \neq s, t \\ \sum_{e \text{ out of } s} x_e &= 1 && \text{for source } s \\ \sum_{e \text{ into } t} x_e &= 1 && \text{for destination } t \\ 0 \leq x_e &\leq 1 && \text{for each edge } e, \end{aligned}$$

where  $x_e$  is the flow on edge  $e$ .

The exact algorithm projects the polytope  $P$  onto the 2-dimensional plane spanned by the distance and loss vectors  $d, \ell$  and enumerates extreme points of the 2D-polytope projection. The smoothed bound below implies that when the distances and losses  $d, \ell$  are perturbed slightly, then the number of extreme points on the 2D-polytope projection is polynomial in expectation with respect to the perturbation. We use the following perturbation and theorem from [13] that applies directly to our problem.

**DEFINITION 1 (PERTURBATION [13]).** *For any  $\rho > 0$  and any unit vector  $u$ , we define a  $\rho$ -perturbation of  $u$  to be a random unit vector  $v$  chosen as follows:*

- 1) Randomly select an angle  $\theta \in [0, \pi]$  from the exponential distribution of expectation  $\rho$ , restricted to the range  $[0, \pi]$ .
- 2) Choose  $v$  uniformly at random from the set of vectors that make an angle of  $\theta$  with  $u$ .

The smoothed bound in the theorem below states that the expected number of extreme points of the projection of the feasible polytope  $P$  onto the perturbed plane spanned by vectors  $v_1, v_2$  is polynomial: The smoothed bound on the number of extreme points is given in the following theorem:

**THEOREM 7 (SMOOTHED BOUND [13]).** *Let  $u_1$  and  $u_2$  be arbitrary unit vectors and denote  $U = \text{span}(u_1, u_2)$ . Let  $V = \text{span}(v_1, v_2)$  be an arbitrary 2-plane. Let  $v_1$  and  $v_2$  be  $\rho$ -perturbations of  $u_1$  and  $u_2$ , respectively, and let  $V = \text{span}(v_1, v_2)$ . The expected number of edges of the projection of  $P$  onto  $V$  is at most  $4\pi\sqrt{2m}/\rho$ , for  $\rho < 1/\sqrt{m}$ .*

There is a tradeoff between the size of the perturbation and the bound in the theorem—the smaller the perturbation, the larger the bound on the expected number of extreme points. However, if we set  $\rho = \frac{1}{\sqrt{2m}}$ , for example, we get the bound  $8\pi m$ , which is linear in the number of edges  $m$ . By the one-to-one correspondence between extreme points on the 2D-polytope projection and breakpoints in the parametric shortest paths problem, the smoothed bound above implies the expected polynomial complexity of the exact algorithm, as stated in the following corollary:

**COROLLARY 8.** *If the edge weight vectors  $d, \ell \in \mathbb{R}^m$  are fixed vectors and  $d', \ell' \in \mathbb{R}^m$  denote their  $\rho$ -perturbations, then the expected number of extreme points on the path polytope shadow on  $\text{span}(d', \ell')$  is linear in the number of graph edges  $m$  and consequently the  $n^{\Theta(\log n)}$  exact algorithm for the dominant path problem has expected polynomial running time.*

This Corollary is the formal statement of Theorem 7.

## 7 FUTURE WORK

This paper focuses on algorithm design, not algorithm engineering. Although our prototype implementation is reasonable, it has not been highly engineered for speed. We could accelerate it by pruning edges of  $G_1$  above some loss threshold, handling measurement points outside the main Dijkstra loop and priority queue, tuning data structures, cache optimization, etc. After such improvements, a careful "horserace" running time comparison against tree-search dominant path codes might be appropriate. The current paper instead focuses on proving the GP algorithm's viability, owing to its already-fast running time and superb fidelity to the exact IDP model.

For simplicity, we focused on the 2D indoor dominant path model, but the outdoor and mixed models are also important. It would be interesting to apply the GP algorithm to these models, and also to 3D models. Finally, we hope that our methods will be integrated into wireless network planning tools, to support AP placement optimization as described in Section 1.

## 8 ACKNOWLEDGMENTS

This paper is dedicated to our late co-author David S. Johnson, an exemplary friend, mentor, and human being. This work was partially supported by NSF through grants CCF-1216103, CCF-1331863, CCF-1350823 and CCF-1733832. Mikkel Thorup's research is supported by his Advanced Grant DFF-0602-02499B from the Danish Council for Independent Research and by his Investigator Grant 16582, Basic Algorithms Research Copenhagen (BARC), from the VILLUM Foundation.

## REFERENCES

- [1] Altair. 2016. Altair Acquires WinProp and AWE Communications GmbH. Retrieved March 16, 2017 from [http://www.altair.com/newsdetail.aspx?news\\_id=11249&news\\_country=en-US](http://www.altair.com/newsdetail.aspx?news_id=11249&news_country=en-US)
- [2] Altair. 2016. WinProp Software for Wave Propagation and Radio Planning. Retrieved March 16, 2017 from <http://www.altairhyperworks.com/product/FEKO/WinProp-Propagation-Modeling>
- [3] Alexander Aschrafi, Philipp Wertz, Michael Layh, Friedrich M. Landstorfer, Gerd Wölfle, and René Wahl. 2006. Impact of Building Database Accuracy on Predictions with Wave Propagation Models in Urban Scenarios. In *Proceedings of IEEE Vehicular Technology Conference, VTC*. 2681–2685.
- [4] Ahmad Awada, Ekkehard Lang, Olaf Renner, Karl-Josef Friederichs, Swen Petersen, Kerstin Pfaffinger, Benjamin Lembke, and Roland Brugger. 2016. Field Trial of LTE eMBMS Network for TV Distribution: Experimental Results and Analysis. *IEEE Transactions on Broadcasting* (2016).
- [5] Patricia J. Carstensen. 1983. *The complexity of some problems in parametric linear and combinatorial programming*. Ph.D. Dissertation. Mathematics Dept., U. of Michigan, Ann Arbor, Michigan.
- [6] CelPlan Wireless Global Solutions. 2017. CellTrace: Indoor Prediction Tools Based on Ray Tracing. Retrieved December 18, 2017 from <http://www.celplan.com/products/celltrace.asp>
- [7] Leonard Grokop, Chirag Patel, Mehmet Yavuz, and Sanjiv Nanda. 2010. SimTown: RF Propagation Models for Urban Femtocell Environments. *Qualcomm White Paper* (2010).
- [8] Daniel Mier Gusfield. 1980. *Sensitivity Analysis for Combinatorial Optimization*. Ph.D. Dissertation. University of California, Berkeley. AAI8029414.
- [9] iBwave. 2007. iBwave Integrates AWE Communications Propagation Module into iBwave Design. Retrieved December 18, 2017 from <http://www.ibwave.com/media-and-events/press-releases/215/ibwave-integrates-awe-communications-propagation-module-into-ibwave-design>
- [10] Jon Kleinberg and Éva Tardos. 2005. *Algorithm Design*. Pearson.
- [11] Farhad Meshkati, Yi Jiang, Lenny Grokop, Sumeeth Nagaraja, Mehmet Yavuz, and Sanjiv Nanda. 2009. Mobility and capacity offload for 3G UMTS femtocells. In *IEEE GLOBECOM 2009*. 1–7.
- [12] Evdokia Nikolova. 2010. Approximation algorithms for reliable stochastic combinatorial optimization. In *APPROX-RANDOM*. Springer-Verlag, 338–351.
- [13] Evdokia Nikolova, Jonathan A. Kelner, Matthew Brand, and Michael Mitzenmacher. 2006. Stochastic Shortest Paths via Quasi-convex Maximization. In *Lecture Notes in Computer Science 4168 (ESA 2006)*. Springer-Verlag, 552–563.
- [14] David Plets, Wout Joseph, Kris Vanhecke, Emmeric Tanghe, and Luc Martens. 2012. Coverage prediction and optimization algorithms for indoor environments. *EURASIP J. Wireless Comm. and Networking* 2012 (2012), 123.
- [15] James A. Sethian. 1999. *Level Set Methods and Fast Marching Methods: Evolving Interfaces in Computational Geometry, Fluid Mechanics, Computer Vision, and Materials Science*. Cambridge University Press.
- [16] The Internet Archive. 2008. WinProp Customers. Retrieved December 14, 2017 from <https://web.archive.org/web/20080509165734/http://www.awe-communications.com/Company/CustomersCommercial.html>
- [17] Gerd Wölfle and Friedrich M. Landstorfer. 1997. Field strength prediction with dominant paths and neural networks for indoor mobile communication. In *MIOP, Mikrowellen und Optronik, 9. Kongreßmesse für Hochfrequenztechnik, Funkkommunikation und elektromagnetische Verträglichkeit*, 216–220.
- [18] Gerd Wölfle and Friedrich M. Landstorfer. 1998. Dominant paths for the field strength prediction. In *Proceedings of the 48th IEEE Vehicular Technology Conference (VTC)*. Ottawa, 552–556.
- [19] Gerd Wölfle, Rene Wahl, Philipp Wertz, Pascal Wildbolz, and Friedrich Landstorfer. 2005. Dominant path prediction model for indoor scenarios. In *German Microwave Conference (GeMIC)*. Ulm, Germany, 176–179.